Research Square

Preprints are preliminary reports that have not undergone peer review.
They should not be considered conclusive, used to inform clinical practice,
or referenced by the media as validated information.

Multimodal imaging features of intra-parenchymal schwannoma

Jiaying Gong
gongjy3@mail.sysu.edu.cn

the Sixth Affiliated Hospital, Sun Yat-sen University

Zelan Ma
the Second Affiliated Hospital of Guangzhou University of Chinese Medicine

Yan Deng
Huashan Hospital, Fudan University

Qianwen Guan
Huizhou Central People's Hospital

Zhongwen Zhou
Huashan Hospital, Fudan University

Shukun Liao
the First Affiliated Hospital of Gannan Medical University

Ke Sun
Huashan Hospital, Fudan University

Na Shen
Tengchong People's Hospital

Donghui Gan
Nanning Fourth People's Hospital

Hanqiu Liu
Huashan Hospital, Fudan University

Research Article

Keywords: Intra-parenchymal schwannoma, imaging features, diffusion weighted imaging, magnetic resonance spectroscopy, perfusion

Posted Date: July 7th, 2026

DOI: https://doi.org/10.21203/rs.3.rs-9972749/v1

License: This work is licensed under a Creative Commons Attribution 4.0 International License. Read Full License

Additional Declarations: No competing interests reported.

Abstract

Purpose

To analyze the CT and MRI features of patients with intra-parenchymal schwannoma.

Methods

The comprehensive CT and MRI features of 22 cases with intra-parenchymal schwannoma were analyzed retrospectively.

Results

There were thirteen men and nine women (median age, 40 years) in this study. The median tumor size was 4.0 cm. Most of the masses located supratentorial. All tumors were well-circumscribed, cystic and solid in 17 cases, solid in four cases and cystic in one case. Hemorrhage in the mass could be observed in two cases, nodular calcification was observed in four cases, and peritumoral edema could be observed in the majority of the cases (n = 15). Most of these lesions (n = 13/16) presented low density on CT plain scan, iso-hypointensity on T1WI and iso-hyperintensity on T2WI. The solid part of the lesion shows unrestricted diffusion in most of the cases. After contrast administration, all masses illustrated heterogeneously moderate to marked enhancement and high perfusion with an elevated ratio of maximum relative cerebral blood volume with a value of 10.5. Six cases underwent MRS examination, choline (Cho) peak was slightly elevated, while N-acetyl aspartate (NAA) peak was not shown or significantly decreased. The Cho/NAA ratio ranged from 0.5 to 2.1.

Conclusion

A well-defined solid and cystic mass with obvious edema, significant and uneven enhancement, low density on CT, unrestricted diffusion, and high perfusion in the contrast-enhancing part, which with a very low or absent NAA peak and slightly elevated Cho and MI peak on MRS, should take into consideration of intra-parenchymal schwannoma.

Introduction

Schwannoma is a tumor that originates from Schwann cells of nerves, accounting for approximately 5%-8% of intracranial tumors [1]. It mostly occurs singularly and originates from cranial nerves, with vestibular nerve origin as the most common. It is characterized by space-occupying lesions in the cerebellopontine angle region, making up about 90% of intracranial schwannomas [2]. Unrelated to cranial nerves, such as intra-parenchymal schwannoma, it is extremely rare for our routine clinical practice [3]. Since Gibson et al. reported the first case of temporal lobe schwannoma in 1966 [4], more than 100 cases of primary schwannomas in the brain parenchyma have been reported successively around the world [3, 5, 6].

Analyzing previous cases, most of them were reported as individual cases, with a very high misdiagnosis rate as meningioma, glioma or hemangioma [7, 8]. Due to their cystic changes, peritumoral edema and obvious enhancement, they were more likely to be misdiagnosed as malignant tumors, causing great psychological burden on patients. With the development of medical imaging technology, functional imaging methods, such as diffusion weighted imaging (DWI), perfusion weighted imaging (PWI), and magnetic resonance spectroscopy (MRS) imaging, can provide more assistance for the diagnosis and differential diagnosis of diseases [9, 10]. However, it is still unknown about the comprehensive characteristics of DWI, PWI and MRS of intra-parenchymal schwannoma. Little advancement has been made to further the understanding and management of these tumors. The available literatures consisted of case reports and small samples that presented variable conventional CT and/or MRI imaging features, lacking comprehensive CT and functional MRI features distinguishing these unusual lesions.

This article will analyze the schwannomas in the brain parenchyma admitted to the hospital, summarize their clinical and imaging features, especially the relevant functional imaging features of DWI, PWI and MRS, also provided the review of the literature, in order to improve the accuracy of diagnosis and increase the understanding of these rare tumors. To our knowledge, this is the first report of relatively large-scale cases of comprehensive CT and functional MRI including DWI, PWI and MRS findings for intra-parenchymal schwannoma.

Materials and methods

Patients

This retrospective study was approved by the institutional review board of our hospital, with the requirement for informed consent waived. From January 2014 to September 2025, intra-parenchymal schwannoma at our hospital were surgically and pathologically proved based on the clinical trials of 22 patients. Fourteen patients underwent CT and MRI examination, seven patients had undergone MRI, while the remaining one patient underwent CT. Clinical and radiologic data were collected for further analysis.

Imaging techniques

The head CT examination was performed with a 256-detector volume CT system (GE Medical Systems, USA) or dual-source CT (Siemens, Germany). MRIs were obtained with 3.0T MR system (Singa Architect [GE Medical Systems, USA] or United 790, China), and 8 channel head coil was adopted. The sequences included sagittal T2-weighted images (T2WI), axial T2- fluid attenuated inversion recovery (FLAIR) sequence, transverse T1/T2-weighted images and axial DWI sequence with b value of 1000 s/mm². Single Section 3D multivoxel ^{1}H-MRS was acquired using a point resolved spectroscopy sequence with water suppression by a chemical shift imaging pulse. Contrast-enhanced sagittal, coronal, and transverse T1-weighted enhanced (T1WI) images were obtained after an intravenous injection of Gadobutrol (Gadovist [Schering, Berlin, Germany]) at a dose of 0.1 mmol/kg and rate of 1.5 ml/second. Dynamic susceptibility contrast perfusion MRI (DSC-MRI) was obtained with gradient echo-echo planar imaging sequence following an intravenous bolus of Gadobutrol at a dose of 0.1 mmol/kg and rate of 4 ml/second using a power injector, followed by the same volume of saline flush. The parameters of DSC-MRI sequence were as follows: plane, axial; repetition time, 1500 ms; echo time, 30 ms; number of excitations, 1; slice thickness, 4 mm; slice increment, 0 mm; flip angle, 90°; field of view, 240 mm; matrix, 128 × 128; dynamic measurements, 60; total acquisition time, 90 seconds.

Imaging data analysis

The images were analyzed by two radiologists with respective 12 and 8 years of experience in the brain imaging. CT or MR characteristics of the imaging data, including location, shape and size, margin, attenuation, enhancement pattern and DWI characteristics were independently evaluated. The analyses of the spectral dataset were performed with the Function Tool of GE 3.0 T workstation (ADW4.7). The distribution maps of different metabolites were obtained, and then distribution maps and MRI images were fused to obtain ^{1}H-MRS curves. The software automatically conducted phase, frequency coding and baseline correction for the spectrum. The built-in software of MRI scanner automatically conducted the baseline calibration, signal average and metabolite identification, and measured the peak area of the tumor, N-acetyl aspartate (NAA), choline (Cho), myoinositol (MI) and creatine (Cr), and calculated the ratio of Cho/NAA. Each spectrum was evaluated for the peak area of NAA at 2.02 ppm, Cho at 3.22 ppm, mI at 3.0 ppm and Cr at 3.03 ppm. DSC-MRI analysis was automatically computed using the model of arterial input function (AIF). The corresponding attenuation time curves that demonstrated a rapid increase in attenuation with sharp peaks were used for analysis. Relative cerebral blood volume (rCBV) maps were generated with the use of voxel-wise division of the area under the concentration-time curve by the area under the AIF. Regions of interest were placed on the solid components of tumors with reference to axial postcontrast T1WI. Voxel placements for spectroscopy and all data analyses were carried out by a trained radiologist who was blind to each subject diagnosis. Any discrepancy was resolved by consensus.

Results

Clinical information

The study group was formed by 13 men and 9 women with a median age of 40 years (range, 12–67 years). Clinical symptoms included headache (6 cases), dizziness (2 cases), headache and dizziness (1 case), headache accompanied by others (2 cases: fluency disorder, change of character), dizziness accompanied by others (4 cases: diminution of vision, visual rotation, intermittent convulsions, facial paralysis), epilepsy (2 cases), photis (1 case), blurred vision (1 case), hypomnesis (1 case), dizziness and vomiting (1 case), accidental findings (1 case).

Imaging findings

In our study, 14 patients underwent CT and MRI examination, six patients had undergone MRI, the remaining two patients underwent CT. The median tumor size was 4.0 cm (range, 1.1–6.5 cm). The masses were respectively, round in five cases (22.7%), lobulated in seven cases (31.8%) and oval in ten case (45.5%). All tumors were well-circumscribed, cystic and solid in 17 cases (77.3%), solid in four cases (18.2%) and cystic in one case (4.5%). Nodular calcification was observed in four cases (18.2%) (Fig. 1), hemorrhage in the mass could be observed in two cases (9.1%) (Fig. 2), and peritumoral edema (n = 15, 68.2%) or cystic alterations could be observed in the majority of the cases (Fig. 1–2). Most of these lesions (n = 13/16) presented low density on CT plain scan, iso-hypointensity on T1-weighted images and iso-hyperintensity on T2-weighted images. In addition, fluid-fluid level was observed in three cases (Fig. 2). The solid part of the lesion shows unrestricted diffusion on DWI in most of the cases (Fig. 1–3). After contrast agents' injection, all masses illustrated heterogeneously moderate to marked enhancement (Fig. 1–3) and high perfusion (Fig. 3) on DSC-MRI showing a rCBV of 10.5 with a curve of leakage. Six cases underwent MRS examination, Cho and MI peak was slightly elevated, while NAA peak was not shown or significantly decreased. The Cho/NAA ratio ranged from 0.5 to 2.14 (Fig. 3). For a detailed summary of the clinical and CT/MR imaging features of 22 patients with intra-parenchymal schwannoma, please refer to Table 1.

Table 1
CT and MRI Imaging Features of 22 cases with intra-parenchymal schwannoma

Case	site	gender	age (years)	modality	texture	cal	hem	density	T1WI	T2WI	DWI	MRS	edema	enhancement
1	R temporal lobe	F	26	CT + MR	cystic and solid	-	+	hypo	iso-hypo	hyper	hypo	/	+	+
2	R temporal lobe	M	58	MR	cystic and solid	-	-	/	/	/	hypo	/	+	+
3	L temporal lobe	F	44	MR	cystic and solid	-	-	/	iso-hypo	hyper	hypo	NAA↓, Cho↑, Cho/NAA 2.06	+	+
4	L temporal lobe	F	56	MR	cystic and solid	-	-	/	/	hyper	hypo	/	+	+
5	L temporal lobe	M	56	MR	cystic and solid	-	-	/	iso-hypo	hyper	/	Cho/NAA 0.6	-	+
6	R frontal lobe	M	60	CT + MR	cystic and solid	-	-	hypo	/	/	/	/	+	+
7	R temporal lobe	M	57	CT	cystic and solid	+	-	iso-hyper	/	/	/	/	+	+
8	R frontal lobe	F	33	CT + MR	solid	-	-	hypo	/	hyper	/	NAA↓, Cho↑, MI↑, Cho/NAA 1.03	-	+
9	L frontal lobe	F	44	CT + MR	cystic and solid	-	-	hypo	iso-hypo	hyper	hypo	/	+	+
10	L frontal lobe	F	45	CT + MR	solid	-	+	iso-hyper	iso-hypo	hyper	iso	/		+
11	R frontal lobe	M	16	CT + MR	cystic and solid	+	-	iso-hypo	iso-hypo	hyper	hypo	NAA↓, Cho↑, MI↑, Cho/NAA 1.55	+	+
12	L temporal lobe	M	47	MR	cystic and solid	-	-	/	/	hyper	/	NAA↓, Cho↑, Cho/NAA 2.14	+	+
13	R frontal lobe	M	31	CT + MR	cystic and solid	-	-	hypo	/	hyper	/	/	+	+
14	R temporal lobe	M	12	CT	cystic and solid	+	-	hypo	/	/	/	/	+	+
15	L frontal lobe	M	16	CT + MR	cystic and solid	-	-	hypo	iso-hypo	hyper	/	NAA↓, Cho↑, NAA/ Cho + Cr↓	+	+
16	R parietal lobe	M	30	MR	cystic and solid	-	-	/	hypo	hyper	/	/	-	+
17	R temporal lobe	M	67	CT + MR	cystic and solid	-	-	hypo	iso-hypo	hyper	/	/	-	+
18	R frontal lobe	F	40	CT + MR	solid	-	-	hypo	iso-hypo	hyper	hypo	/	+	+

R: right; L: left; M: male; F: female; cal: calcification; hem: hemorrhage; iso: isodensity/isointensity; hypo: hypodensity/hypointensity; hyper: hyperdensity/hyperintensity; '-' denotes negative; '+' denotes positive; '/' denotes not available. CT: computed tomography; MRI: magnetic resonance imaging; NAA: N-acetyl aspartate; Cho: choline; Cr: creatine.

Case	site	gender	age (years)	modality	texture	cal	hem	density	T1WI	T2WI	DWI	MRS	edema	enhancement
19	R temporal lobe	F	53	CT + MR	cystic and solid	-	-	hypo	hypo	hyper	hypo	/	-	+
20	L temporal lobe	F	35	CT + MR	cystic	+	-	hypo	hypo	hyper	hypo	/	-	+
21	R parietal lobe	M	15	CT + MR	solid	-	-	iso-hyper	/	hyper	/	/	+	+
22	R cerebellar hemisphere	M	55	CT + MR	cystic and solid	-	-	hypo	hypo	hyper	hypo	/	+	+

R: right; L: left; M: male; F: female; cal: calcification; hem: hemorrhage; iso: isodensity/isointensity; hypo: hypodensity/hypointensity; hyper: hyperdensity/hyperintensity; '-' denotes negative; '+' denotes positive; '/' denotes not available. CT: computed tomography; MRI: magnetic resonance imaging; NAA: N-acetyl aspartate; Cho: choline; Cr: creatine.

Surgical and pathological findings

At surgery, all tumors were intra-parenchymal, among which 11 cases were located in the temporal lobe, 8 cases in the frontal lobe, 2 cases in the parietal lobe, and only 1 lesion was located in the subtentorial cerebellar hemisphere. As high as 86.4% (19/22) lesions located on the surface of the brain parenchyma or around the ventricles. The masses were rounded or lobulated, firm, well-defined, with a tan-yellow to greyish-white appearance. All tumors, especially the larger mass, were heterogeneous in texture, with cystic degeneration, calcification and hemorrhage. Microscopically, pathological examination with hematoxylin and eosin staining, cellular areas of spindle-shaped cells and nuclear palisading were present in all cases. This appearance was defined as Antoni A. All tumors had Antoni B areas, which are characterized by the loose texture and polymorphism of tumor cells embedded in a fine honeycomb eosinophilic matrix (Fig. 4). Moreover, the tumors indicated intense immunostaining for S100 and Vimentin and a relatively low Ki67 index (approximately 1–8%), implying that the tumors were neurogenic and the proliferation activity was relatively low.

Discussion

In this study, we studied the imaging characteristics of intra-parenchymal schwannoma which were unrelated to the cranial nerves nerve in 22 cases. They usually manifested as a well-defined solid and cystic mass with obvious edema, significant and uneven enhancement, low density on CT, hypointensity on DWI, and high perfusion in the contrast-enhancing part, which with a very low or absent NAA peak and slightly elevated Cho and MI peak on MRS. Although there have been some reports on this case in the past, this group of cases can bring more comprehensive imaging features of the disease.

Schwannomas in the brain parenchyma refer to schwannomas that occur within the brain tissue and are not related to cranial nerves. They originate from Schwann cells and account for less than 1% of the central nervous system schwannomas treated surgically [5]. This group of cases accounts for 0.63% of the intracranial schwannomas of the same stage in our hospital, which is extremely rare. Search findings from databases such as Pubmed, Web of Science, Chinese National Knowledge Infrastructure, Wanfang, and SinoMed reported the first case of schwannoma in the brain parenchyma in 1966, there have been over 100 reports of 148 cases of schwannomas in the brain parenchyma both at home and abroad [2, 4]. As reported in the previous studies, the origin of this type of tumor remains a subject of academic discussion. Current understanding is merely speculation or hypothesis. Feigin et al. believed that these tumor cells originated from pluripotent mesenchymal cells[11], while Tsuiki et al. suggested that Schwannomas in the brain were the transformation of mesenchymal cells into Schwann cells of the ectoderm within the brain parenchyma, or they may originate from neural crest cells [12]. Ishihara et al. believed that this tumor originated from the nerve plexus around the blood vessels in the brain parenchyma. Some tumors grew along the perivascular space and formed vasogenic edema, which precisely confirmed this hypothesis [13]. Luo et al. believed that this tumor originated from neural stem cells because they were mitotic and had a long lifespan, so they can accumulate sufficient mutations to form tumors [14]. None of the above hypotheses can fully explain its occurrence, development and clinical characteristics. Some scholars even believed that a single theory was not sufficient to explain the occurrence of schwannoma in the brain, which may be caused by several different etiological mechanisms together [15].

Similar to previous reports, there was no gender difference in the patient population reported in this group, with males accounting for 59.1% and females 40.9% [16]. Previous literatures reported that this tumor mostly occurred in adolescents, with a majority occurring before the age of 30 years old [17]. However, in this group of cases, the median age was 40 years old, the minimum age is 12 years old, and the maximum age is 67 years old. The peak age of onset was in the 51–60 age groups. Because intracranial schwannomas were mostly benign tumors, they grew relatively slowly and caused less damage to adjacent brain structures, so symptoms may persist for a long time [18]. As reported in previous studies, epileptic seizures were regarded as the most common symptom. In this group of cases, headache or dizziness was the initial symptom of most cases, followed by epileptic seizures and changes in vision. As expected, the neurologic signs were related to the anatomic location of the lesion. In the earlier research reports, the majority of tumors were located in the temporal and frontal regions, which are more common sites for producing schwannoma-associated seizures [19]. However, the first location in our cases was the temporal lobe, but the most clinical symptoms were headache and/or dizziness, which might be related to the local occupying effect causing rising-intracranial-pressure due to the relatively large lesions [20, 21].

Imaging studies showed that this tumor had several major characteristics, including cystic changes, calcification, peritumoral edema, and was located on the surface of the brain parenchyma or around the ventricles [6, 22]. It was reported that the cystic change rate of this tumor can be as high as 88% [23]. Similar to the literature reports, the cystic change rate of this group was 82% (18/22), which was much higher than the 20% of acoustic neuroma. It may be related to

the necrosis and apoptosis of cells in the tumor center and peritumoral edema. The cyst walls of these tumors were smooth, and the cystic areas were regular. Compared with peripheral schwannomas, there was no significant difference in histological immunohistochemistry of in intra-parenchymal schwannomas. They were composed of two main microscopic components named Antoni A areas (a highly cellular component) and Antoni B areas (a myxoid component) [24], which correlated well with imaging findings of cystic and solid tumors. We could also observe peritumoral cystic alterations apart from the cystic change within the tumor, which may be related to an obstruction of cerebrospinal fluid flow secondary to the peritumoral adhesions [25].

Peritumoral edema was relatively common in intra-parenchymal schwannoma. In the previous reports, at least half of the cases presented with peritumoral edema, and the imaging manifestation was angioedema [8, 13, 26]. The rate of peritumoral edema in this group of cases was as high as 68% (15/22). However, edema caused by peripheral schwannomas was rare according to literatures, which can become one of the important imaging features of intra-parenchymal schwannoma. Although calcification was uncommon in schwannomas, some scholars believed that calcification was an important feature of intra-parenchymal schwannomas [27, 28]. Although calcification occurred in less than 30% of cases, its incidence was much higher than that of peripheral schwannomas such as acoustic neuromas. Although only four cases in this group showed calcification, it can still provide clues for a correct diagnosis. Besides, we also observed some uncommon imaging findings, such as hemorrhage, lobulation and fluid-fluid level in some cases in this study.

Unlike previous studies, we provided the DWI, PWI and MRS characteristics of some cases. DWI has been used for characterization of tumor cellularity and unique microstructure, and increasingly applied for tumor differentiation and evaluation of treatment effects [29]. Ota et. al assessed the role of DWI to differentiate schwannomas and metastases in the cerebellopontine angles, with the cutoff values of normalized mean apparent diffusion coefficient (ADC) ratio 1.68 [30]. In this study, the normalized mean ADC ratio was 1.78, similar to the previous studies, which might contribute to the larger likely to undergo cystic changes of schwannomas and generally high cellularity of other malignant tumors [31]. But there was no significant difference in ADC in distinguish meningioma, paraganglioma, and schwannoma in the head and neck [32]. As for the signal, there was no restriction on DWI in almost all cases, similar findings were described by other scholars in schwannomas related to cranial nerves [33]. The possible reason was that there was no significant difference in histological immunohistochemistry of intra-parenchymal schwannomas compared with intracerebral and peripheral schwannomas.

DSC-MRI technique can provide physiologic information regarding tumor's vascular permeability and microvasculature, rCBV was the most commonly used parameter for tumor grading, brain tumor differentiation, and treatment response assessment [29]. Our patient showed high rCBV with a characteristic curve exhibiting only partial recovery of the signal intensity loss due to immediate and persistent leakage of contrast agent related to the complete absence of the blood brain barrier. This type of perfusion curve has been widely described in extra-axial lesions as in meningiomas and schwannomas located in the cerebellopontine angle [34]. The intra-parenchymal schwannomas in our cohort were typically hypervascular, consistent with previous literatures about peripheral and cranial schwannomas confirmed by dynamic-contrast enhanced MRI (DCE-MRI) and arterial spin labeling [35]. Schouten et. al found higher mean K^{trans} and lower mean v_e tumor values were strongly associated with vestibular schwannomas growth by DCE-MRI. Consistent with nerve-originated schwannomas, intra-parenchymal schwannomas showed time-intensity curve with rapid wash-in followed by continuous slower wash-in without washout which can be explained by the increased permeability to the extravascular extracellular space caused by the small thin-walled blood vessels [36]. In this study, although DSC-MRI could not support significant difference between intra-parenchymal schwannomas and other benign and/or malignant tumors, when conventional imaging was indecisive for differentiation of the other tumors, adding DSC-MRI could be helpful for tumor differentiation.

MRS can provide information related to cell membrane proliferation, neuronal damage, energy metabolism, and necrotic transformation of brain or tumor tissues. MRS gives information at the molecular level rather than structural and anatomic imaging of tissues and organs by identifying various chemical metabolites, such as Cho, Cr, MI and NAA. MRS metabolite ratios can differentiate between the non-neoplastic and neoplastic lesions, benign and malignant brain lesions [37]. However, there was little information about the spectroscopic signatures of intra-parenchymal schwannomas. We found slightly elevated Cho peak, significantly decreased or absent NAA peak, low Cho/NAA ratio within the intra-parenchymal schwannomas, and elevated MI peak was observed in one case with long echo-time MRS. Similar findings were observed in vestibular schwannoma [38]. Paredes et. al also found elevated Cho and MI in the intra-parenchymal schwannomas, but the NAA peak was also elevated, probably due to they adopted single voxel spectroscopy with short echo-time including normal brain tissue [39]. The absence of the NAA peak suggested the intra-parenchymal schwannomas were unrelated to gliocyte, which can be used as a potential tool to distinguish between glial and non-glial origin.

Since intra-parenchymal schwannomas have no specific manifestations, although some or all of the above-mentioned characteristics have appeared in previous cases, and due to the features of cystic change, peritumoral edema, and marked heterogeneous enhancement, almost all of our cases were misdiagnosed as gliomas or meningiomas before surgery. Most of cases were diagnosed as high-grade gliomas before surgery, which undoubtedly increased the psychological burden on patients or their families. Fortunately, although the vast majority of reported cases were misdiagnosed as gliomas or meningiomas, the first-choice treatment for this tumor was surgery. The surgical treatment has achieved good results, with a low incidence of postoperative complications and a favorable prognosis. In daily work, when encountering other tumors such as ganglioglioma, pilocytic astrocytoma, pleomorphic xanthoastrocytoma, ependymoma within the brain parenchyma, cystic meningioma and dysembryoplastic neuroepithelial tumor, with hemorrhage and/or calcification, cystic change, peritumoral edema and obvious heterogeneous enhancement, differential diagnosis with intra-parenchymal schwannoma should also take into consideration.

However, this study still has some limitations. First, the number of participants in this research was not large enough. Second, this was a retrospective study, although the research methods in the cases were relatively comprehensive, not all patients underwent the same examinations and advanced MRI techniques, the observed imaging features may be just a kind of tendency or phenomenon, which should be further supported by the evidence from large-scale case study. Finally, there was a wide variety of examination machines and imaging techniques. Whether these features were specific to intra-parenchymal schwannomas or were affected by imaging techniques remains unclear. In the future, more clinical studies with larger sample sizes and multicenter should be encouraged to evaluate the significance of each advanced MRI technique and the specificity and sensitivity of each radiological parameter.

Conclusion

In conclusion, intra-parenchymal schwannomas ware rare and difficult to diagnose. They commonly had the following imaging manifestations: The patients were generally younger in age. They were more common in males and mostly located in the superficial parts of the supratentorial brain or around the ventricles. A well-defined solid and cystic mass with obvious edema, significant and uneven enhancement, low density on CT, unrestricted diffusion on DWI, and high perfusion in the contrast-enhancing part, which with a very low or absent NAA peak and slightly elevated Cho and MI peak on MRS, should take into consideration of intra-parenchymal schwannoma. The final diagnosis of this disease should be combined with pathological and immunohistochemical findings.

Declarations

Declaration of competing interest

The authors declare that they have no competing interests.

Ethics approval and consent to participate

This study was approved by the Institutional Ethics Review Board of Huashan Hospital, Fudan University (no. 2025 – 1052)

Funding

This study was supported by the National Natural Science Foundation of China (82371935).

Author Contribution

H.Q.L: Investigation, Supervision. J.Y.G and Z.L.M: Data analyzed and interpreted, Writing original formal manuscript. Y.D, Q.W.G, Z.W.Z., S.K.L, N.S and D.H.G: data acquisition and analysis. K.S., Contributed to Methodology. All authors read and approved the final manuscript.

Data availability

The data that support the findings of this study are available from the corresponding author upon reasonable request.

References

1. Gao Y, Qin Z, Li D et al (2018) Intracerebral schwannoma: a case report and literature review. Oncol Lett 16(2):2501–2510. https://doi.org/10.3892/ol.2018.8949
2. Jiang N, Pan Z, Chen Y et al (2024) Analysis of the clinical characteristics of schwannomas in the ventricles and brain parenchyma. Int J Neurol Neurosurg 51(3):45–54
3. Zhang Z, Mo Z, Zhang Y et al (2022) CT and MRI findings of intra-parenchymal and intra-ventricular schwannoma: a series of seven cases. BMC Med Imaging 22(1):197. https://doi.org/10.1186/s12880-022-00917-z
4. Gibson AA, Hendrick EB, Conen PE (1966) Case reports. Intracerebral schwannoma. Report of a case. J Neurosurg 24(2):552–557. https://doi.org/10.3171/jns.1966.24.2.0552
5. Agarwal P, Garcia M, Barr L et al (2023) Intracerebral schwannoma in a pediatric patient with schwannomatosis: a case report and literature review. Pediatr Blood Cancere30483. https://doi.org/10.1002/pbc.30483
6. Zagardo MT, Castellani RJ, Rees JH et al (1998) Radiologic and pathologic findings of intracerebral schwannoma. AJNR Am J Neuroradiol 19(7):1290–1293
7. Zhang Q, Feng X, He H et al (2007) Multi-slice helical CT perfusion imaging in evaluating intracranial neoplasms and tumor-like lesions. Zhonghua zhong liu za zhi [Chinese journal of oncology] 29(2):131–135
8. Takei H, Schmiege L, Buckleair L et al (2005) Intracerebral schwannoma clinically and radiologically mimicking meningioma. Pathol Int 55(8):514–519. https://doi.org/10.1111/j.1440-1827.2005.01862.x
9. Jaskólski DJ, Fortuniak J, Stefańczyk L et al (2013) Differential diagnosis of intracranial meningiomas based on magnetic resonance spectroscopy. Neurol Neurochir Pol 47(3):247–255. https://doi.org/10.5114/ninp.2013.32998
10. Schouten SM, Lewis D, Cornelissen S et al (2025) Dynamic contrast-enhanced and diffusion-weighted MR imaging for predicting tumor growth of sporadic vestibular schwannomas: a prospective study. Neuro Oncol 27(4):1116–1127. https://doi.org/10.1093/neuonc/noae252
11. Feigin I, Ogata J (1971) Schwann cells and peripheral myelin within human central nervous tissues: the mesenchymal character of schwann cells. J Neuropathol Exp Neurol 30(4):603–612. https://doi.org/10.1097/00005072-197110000-00005
12. Tsuiki H, Kuratsu J, Ishimaru Y et al (1997) Intracranial intraparenchymal schwannoma: report of three cases. Acta Neurochir (Wien) 139(8):756–760. https://doi.org/10.1007/BF01420049

13. Ishihara M, Miyagawa-Hayashino A, Nakashima Y et al (2009) Intracerebral schwannoma in a child with infiltration along perivascular spaces resembling meningioangiomatosis. Pathol Int 59(8):583–587. https://doi.org/10.1111/j.1440-1827.2009.02410.x
14. Luo W, Ren X, Chen S et al (2013) Intracranial intraparenchymal and intraventricular schwannomas: report of 18 cases. Clin Neurol Neurosurg 115(7):1052–1057. https://doi.org/10.1016/j.clineuro.2012.10.029
15. Wong S, Moes G, Ernest K et al (2014) Innervation of the brain, intracerebral schwann cells and intracerebral and intraventricular schwannomas. Child's Nerv system: ChNS: official J Int Soc Pediatr Neurosurg 30(5):815–824. https://doi.org/10.1007/s00381-014-2394-7
16. D'Almeida Costa F, Dias TM, Lombardo KA et al (2020) Intracranial cellular schwannomas: a clinicopathological study of 20 cases. Histopathology 76(2):275–282. https://doi.org/10.1111/his.13967
17. Sharma MC, Karak AK, Gaikwad SB et al (1996) Intracranial intraparenchymal schwannomas: a series of eight cases. J Neurol Neurosurg Psychiatry 60(2):200–203. https://doi.org/10.1136/jnnp.60.2.200
18. Kurtkaya-Yapicier O, Scheithauer B, Woodruff JM (2003) The pathobiologic spectrum of schwannomas. Histol Histopathol 18(3):925–934. https://doi.org/10.14670/HH-18.925
19. Alayyaf M, Taher Nasir N (2019) Seizures and blurred vision as initial presentation of intracerebral schwannoma: a rare tumor of the brain. Case Rep Pathol 20198158950. https://doi.org/10.1155/2019/8158950
20. Flores-Montanez Y, Nahas SJ (2020) Unusual brain MRI findings in patients imaged for headache: a case series. Curr Pain Headache Rep 24(9):51. https://doi.org/10.1007/s11916-020-00881-9
21. Carlson ML, Tveiten ØV, Driscoll CL et al (2015) Risk factors and analysis of long-term headache in sporadic vestibular schwannoma: a multicenter cross-sectional study. J Neurosurg 123(5):1276–1286. https://doi.org/10.3171/2014.12.JNS142109
22. Yazol M, Derinkuyu BE, Boyunaga O (2023) Three different faces of schwannoma in pediatric patients. Curr Med Imaging. https://doi.org/10.2174/1573405620666230414115555. 10-2174
23. Khoo HM, Taki T (2012) Periventricular intraparenchymal schwannoma. Case report. Neurol Med Chir (Tokyo) 52(8):603–607. https://doi.org/10.2176/nmc.52.603
24. Wilson BR, Steinberg JA, Snyder V et al (2016) Histologic evidence for arteriovenous malformation-like vasculature occurring within an intracerebral schwannoma: a case report and review of the literature. https://doi.org/10.1016/j.wneu.2016.05.078. World Neurosurg 92582-589
25. Tali ET, Yuh WT, Nguyen HD et al (1993) Cystic acoustic schwannomas: MR characteristics. AJNR Am J Neuroradiol 14(5):1241–1247
26. Haga Y, Shoji H, Oguro K et al (1997) Intracerebral schwannoma–case report. Neurol Med Chir (Tokyo) 37(7):551–555. https://doi.org/10.2176/nmc.37.551
27. Menku A, Oktem IS, Kontas O et al (2009) Atypical intracerebral schwannoma mimicking glial tumor: case report. Turk Neurosurg 19(1):82–85
28. Ezura M, Ikeda H, Ogawa A et al (1992) Intracerebral schwannoma: case report. Neurosurgery 30(1):97–100. https://doi.org/10.1227/00006123-199201000-00017
29. Ota Y, Liao E, Capizzano AA et al (2022) Intracranial paragangliomas versus schwannomas: role of dynamic susceptibility contrast perfusion and diffusion MRI. J neuroimaging: official J Am Soc Neuroimaging 32(5):875–883. https://doi.org/10.1111/jon.13002
30. Ota Y, Liao E, Zhao R et al (2022) Advanced MRI to differentiate schwannomas and metastases in the cerebellopontine angle/internal auditory canal. J neuroimaging: official J Am Soc Neuroimaging 32(6):1177–1184. https://doi.org/10.1111/jon.13028
31. Surov A, Meyer HJ, Wienke A (2020) Apparent diffusion coefficient for distinguishing between malignant and benign lesions in the head and neck region: a systematic review and meta-analysis. Front Oncol 91362. https://doi.org/10.3389/fonc.2019.01362
32. Ota Y, Liao E, Capizzano AA et al (2022) MR diffusion and dynamic-contrast enhanced imaging to distinguish meningioma, paraganglioma, and schwannoma in the cerebellopontine angle and jugular foramen. J neuroimaging: official J Am Soc Neuroimaging 32(3):502–510. https://doi.org/10.1111/jon.12959
33. Singh K, Singh MP, Thukral C et al (2015) Role of magnetic resonance imaging in evaluation of cerebellopontine angle schwannomas. Indian J Otolaryngol Head Neck Surg 67(1):21–27. https://doi.org/10.1007/s12070-014-0736-0
34. Cebeci H, Kilincer A, Duran Hİ et al (2021) Precise discrimination between meningiomas and schwannomas using time-to-signal intensity curves and percentage signal recoveries obtained from dynamic susceptibility perfusion imaging. J Neuroradiol 48(3):157–163. https://doi.org/10.1016/j.neurad.2020.09.008
35. Li K, Lewis D, Coope DJ et al (2021) The LEGATOS technique: a new tissue-validated dynamic contrast-enhanced MRI method for whole-brain, high-spatial resolution parametric mapping. Magn Reson Med 86(4):2122–2136. https://doi.org/10.1002/mrm.28842
36. Eraky AM, Beck RT, Treffy RW et al (2023) Role of advanced MR imaging in diagnosis of neurological malignancies: current status and future perspective. J Integr Neurosci 22(3):73. https://doi.org/10.31083/j.jin2203073
37. Tamilchelvan P, Boruah DK, Gogoi BB et al (2021) Role of MRI in differentiating various posterior cranial fossa space-occupying lesions using sensitivity and specificity: a prospective study. Cureus 13(7):e16336. https://doi.org/10.7759/cureus.16336
38. Bose A, Prasad U, Kumar A et al (2023) Characterizing various posterior fossa tumors in children and adults with diffusion-weighted imaging and spectroscopy. Cureus 15(5):e39144. https://doi.org/10.7759/cureus.39144
39. Paredes I, Jimenez Roldán L, Ramos A et al (2012) Intraparenchymal schwannomas: report of two new cases studied with MRI and review of the literature. Clin Neurol Neurosurg 114(1):42–46. https://doi.org/10.1016/j.clineuro.2011.07.003

Figures

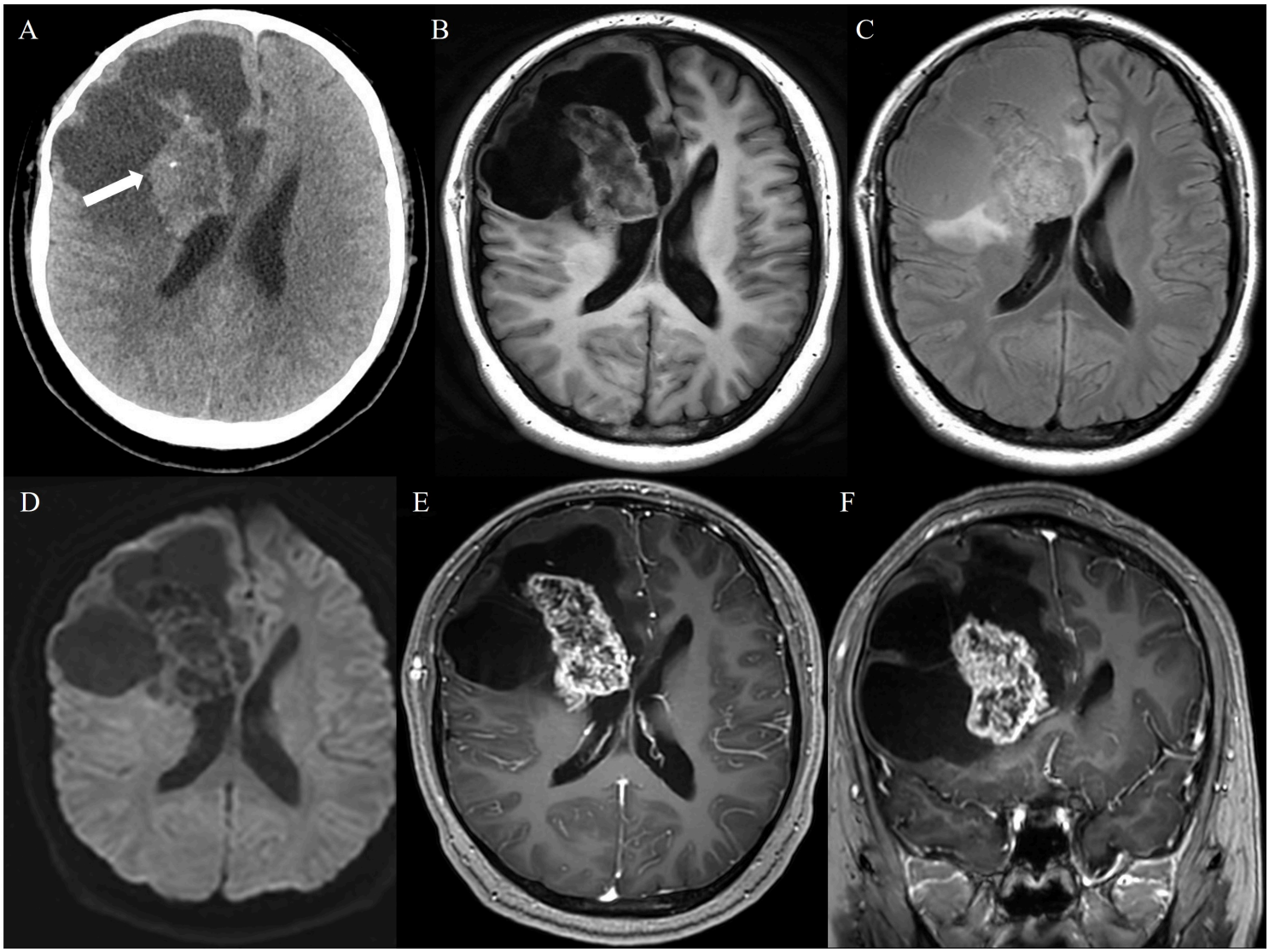


Figure 1

CT and MRI findings of a 16-year-old man with intra-parenchymal schwannoma. On CT plain scan, an iso-hypodense mass with nodular calcification (arrow) was seen in the right frontal lobe, accompanied by obvious perilesional edema (**A**). A well-defined cystic-solid mass with peritumoral edema was observed in the right frontal lobe. The mass showed hypo-intensity on T1WI and hypo-/hyper-intensity on T2-FLAIR (**B** and **C**). The solid part of the lesion showed unrestricted diffusion on DWI (**D**). Heterogeneous and marked enhancement could be observed on the axial and coronal T1WI (**E** and F). CT: computed tomography, MR: magnetic resonance imaging, T1WI: T1-weighted imaging, T2-FLAIR: T2-fluid attenuated inversion recovery, DWI: diffusion weighted imaging.

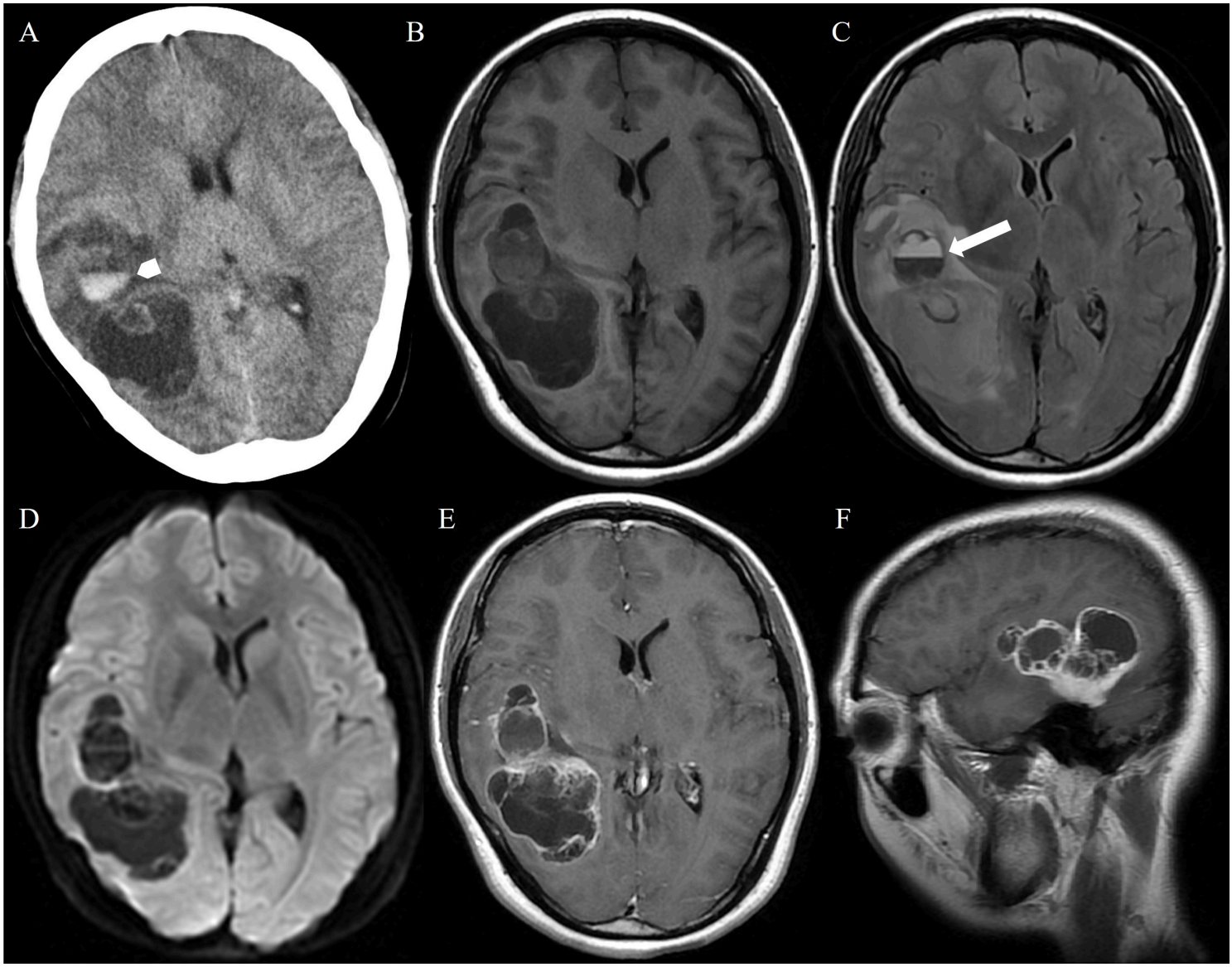


Figure 2

CT and MRI findings of a 26-year-old woman with intra-parenchymal schwannoma. A cystic-solid mixed-density mass was seen in the right temporal lobe, accompanied by high-density hemorrhage (arrow head) within the tumor on unenhanced CT (**A**). A well-defined heterogeneous mass was observed in the right temporal lobe. The mass showed hypo-intensity on T1WI and hyper-intensity on T2-FLAIR (**B** and **C**). Hemorrhage showed slightly high signal on T1WI and low signal on T2-FLAIR, and formed a fluid-fluid level with the cystic component within the mass (arrow). The mass displayed low signal on DWI (**D**). The cyst wall and solid components showed obvious heterogeneous enhancement on the axial and sagittal T1WI (**E** and **F**). CT: computed tomography, MR: magnetic resonance imaging, T1WI: T1-weighted imaging, T2-FLAIR: T2-fluid attenuated inversion recovery, DWI: diffusion weighted imaging.

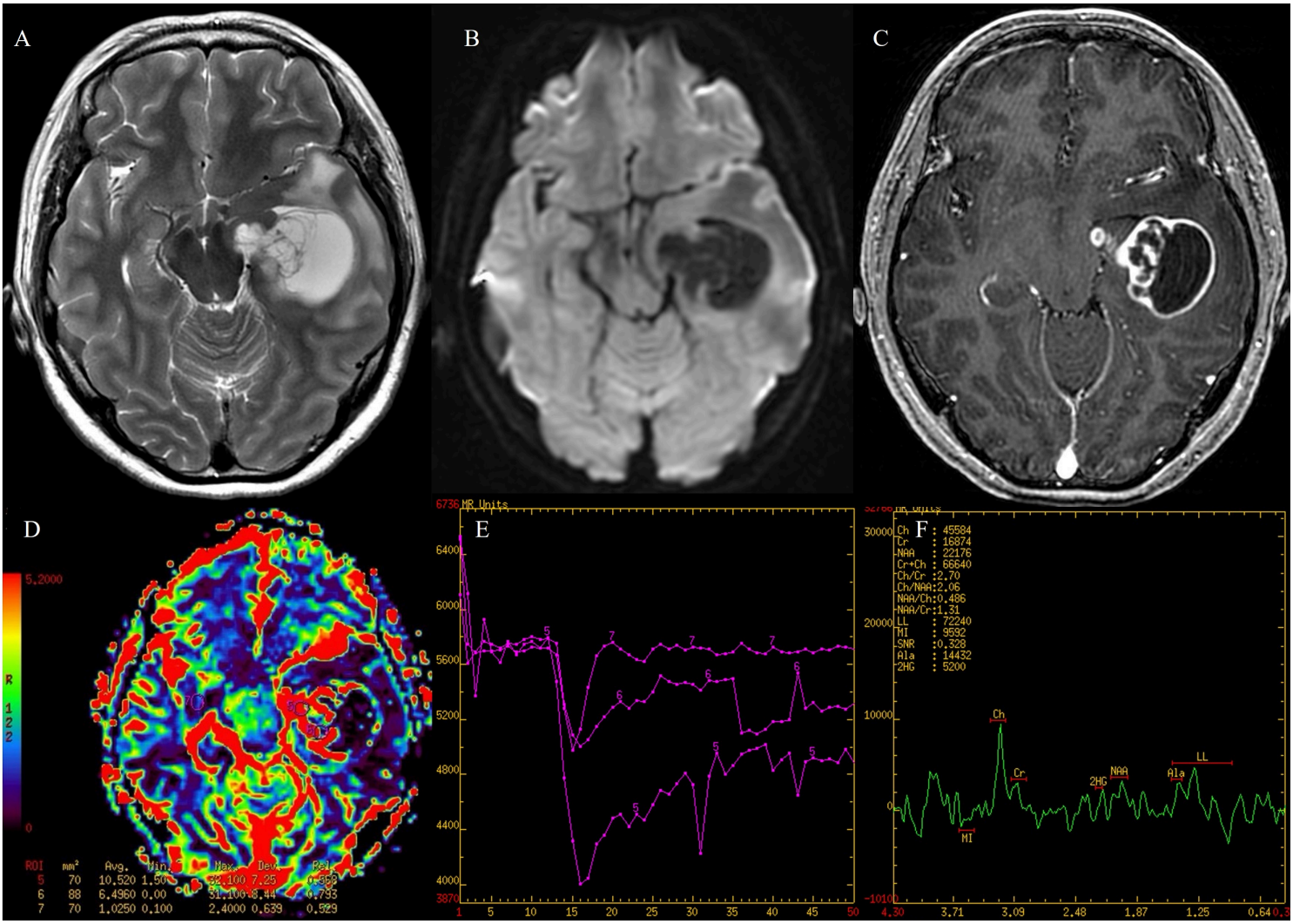


Figure 3

MRI findings of a 44-year-old woman with intra-parenchymal schwannoma. A well-defined cystic-solid heterogeneous mass with septa was observed in the left temporal lobe showed hyper-intensity on T2WI (**A**). There was no restriction on DWI (**B**). The cyst wall, the septa and the solid components showed obvious heterogeneous enhancement on the axial T1WI (**C**). Perfusion study showed the selected voxels demonstrated an elevated ratio of maximum relative cerebral blood volume with a value of 10.5. The intensity-time curve does not return to baseline due to massive leakage (**D-E**). Spectroscopy showed elevated Cho and decreased NAA peak. The Cho/NAA ratio was 2.06 (**F**). T2WI: T2- weighted imaging, DWI: diffusion weighted imaging, Cho: choline, NAA: N-acetyl aspartate.

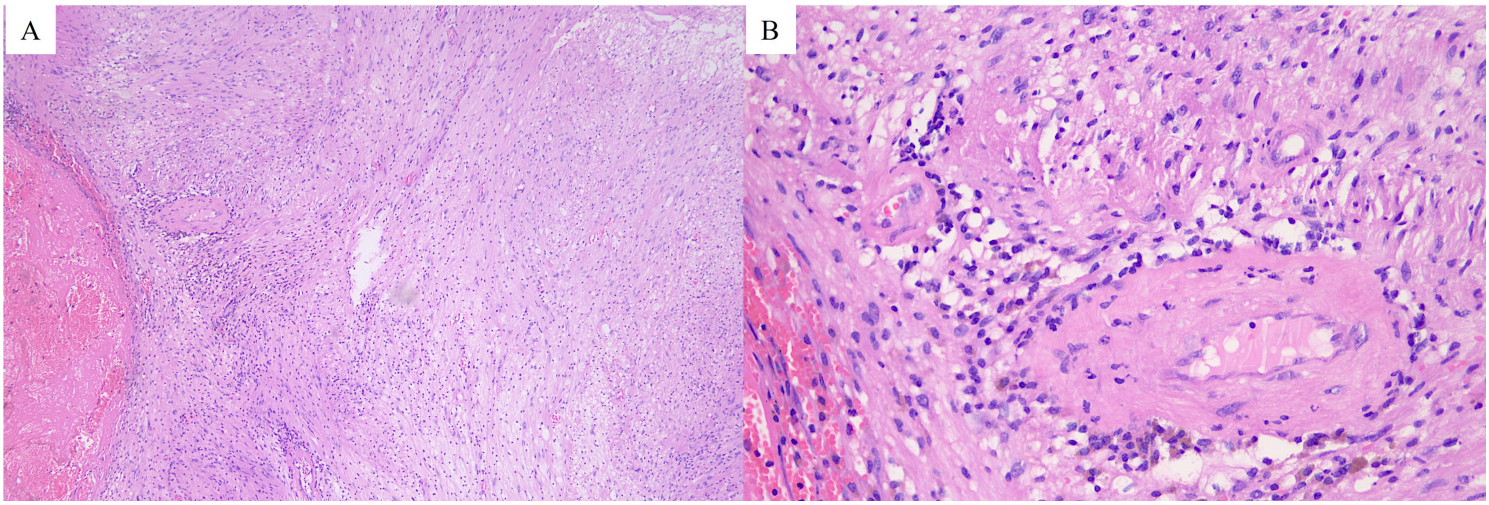


Figure 4

Pathological microscopy showed that spindled cells arranged in short bundles and interlacing fascicles (Antoni A areas), and the loose, myxoid matrix formed Antoni B areas. Patchy hemorrhage and cystic degenerations could be observed (A-B, HE×40, HE×200). HE: hematoxylin-eosin.